Water Resources Research

RESEARCH ARTICLE
10.1029/2024WR039739

Simulating Realistic Design Storms: A Joint Return Period Approach

Tabea Cache[1], Emanuele Bevacqua[2], Jakob Zscheischler[2,3], Hannes Müller-Thomy[4], and Nadav Peleg[1,5]

[1]Institute of Earth Surface Dynamics, University of Lausanne, Lausanne, Switzerland, [2]Department of Compound Environmental Risks, Helmholtz Centre for Environmental Research–UFZ, Leipzig, Germany, [3]Department of Hydro Sciences, TUD Dresden University of Technology, Dresden, Germany, [4]Division of Hydrology and River Basin Management, Leichtweiß Institute for Hydraulic Engineering and Water Resources, Technische Universität Braunschweig, Brunswick, Germany, [5]Expertise Center for Climate Extremes, University of Lausanne, Lausanne, Switzerland

Key Points:

- We propose a method to simulate design storms considering joint return periods across multiple precipitation durations within storms
- The new method can support improved flood risk assessments by providing more realistic design storms and intensity patterns
- The method uses copula and micro-canonical cascade models to simulate extreme precipitation with realistic duration-frequency dependencies

Supporting Information:

Supporting Information may be found in the online version of this article.

Correspondence to:

T. Cache,
tabea.cache@unil.ch

Citation:

Cache, T., Bevacqua, E., Zscheischler, J., Müller-Thomy, H., & Peleg, N. (2025). Simulating realistic design storms: A joint return period approach. *Water Resources Research*, *61*, e2024WR039739. https://doi.org/10.1029/2024WR039739

Received 17 DEC 2024
Accepted 9 JUN 2025

Author Contributions:

Conceptualization: Tabea Cache, Emanuele Bevacqua, Jakob Zscheischler, Nadav Peleg
Formal analysis: Tabea Cache
Funding acquisition: Nadav Peleg
Methodology: Tabea Cache
Resources: Hannes Müller-Thomy, Nadav Peleg
Software: Tabea Cache
Visualization: Tabea Cache
Writing – original draft: Tabea Cache
Writing – review & editing: Emanuele Bevacqua, Jakob Zscheischler, Hannes Müller-Thomy, Nadav Peleg

Abstract Design storms are key components for planning drainage networks and flood risk management. Due to atmospheric processes, precipitation accumulations across multiple temporal intervals are often correlated and can combine to shape flood intensities. However, current design storm guidance overlook the observed correlations between return periods of different duration intervals within storms and may thereby lead to under- or over-estimation of the flood risk. We present a new approach for generating plausible design storms that accounts for joint return periods. Focusing on short-duration extreme precipitation events, potentially leading to urban pluvial flooding, we analyze the dependencies between critical precipitation intensities over the 10-min, 30-min, 1-hr, 3-hr, and 6-hr intervals, for data from Zurich (Switzerland). We then propose a method based on a canonical vine copula model for sampling precipitation intensities that reflect the observations' dependencies. Using this model, we then generate realistic design storms with a constrained micro-canonical cascade model. Our results shows that the common block methods (e.g., the Chicago and Euler design storms) tend to overestimate total precipitation volumes on average, by up to 56%. Furthermore, we highlight the variability in possible duration-frequency profiles, leading to both higher and lower total precipitation volumes compared to standard approaches. This underscores the need to switch from traditional block methods to a more realistic sampling of design storms, incorporating multiple design storm scenarios for robust risk assessment. The model is applicable to any time series of precipitation, regardless of its location or climate. The code is freely available.

Plain Language Summary This study focuses on improving how we simulate design storms. Design storms are used to mimic extreme precipitation events, helping engineers and planners predict the storms that an infrastructure must be able to withstand. However, current methods to derive these storms do not explicitly account for how different precipitation intensities co-occur over different durations within a single precipitation event (e.g., short, intense 10-min bursts or longer, sustained 6-hr rain). This can lead to under- or over-estimation of flood risks. In our research, we looked at how precipitation intensities vary over the time intervals of 10 min, 30 min, 1 hr, 3 hr, and 6 hr during storms. We developed a new model, using statistical methods, to simulate precipitation that better reflects the intensity dependencies observed in measured precipitation events. When compared to a commonly used design storm model, our method resulted in an average reduction in total storm volume by up to 56%. Our method provides a more accurate way to create design storms, which can help improve flood risk assessments.

1. Introduction

Intense short-duration precipitation events can cause catastrophic flooding, particularly in densely populated urban areas (Cristiano et al., 2017; Kundzewicz et al., 2014). A key element of planning flood-resilient cities is the estimation of flood hazard, which is commonly achieved by modeling the flood response for synthetic extreme precipitation events, referred to as design storms (Watt & Marsalek, 2013). Storm drainage networks are thus designed to withstand the flow resulting from design storms that the structure is expected to experience during its lifetime.

Design storms are characterized by specific precipitation intensities over different durations for assigned values of return period. This information is summarized in the intensity-duration-frequency curves (IDF; Chow

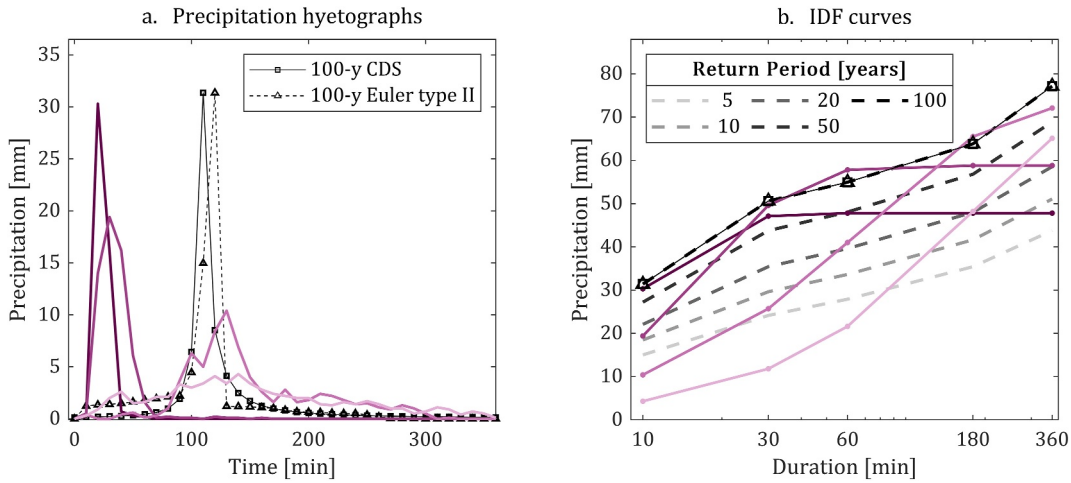

Figure 1. Comparison of (a) hyetographs and (b) return periods across different durations for observed precipitation events (solid purple lines), as well as for the 100-year Chicago design storm (solid square line) and the 100-year Euler type II design storm (dotted triangle line) in Zurich. Dashed lines in (b) represent the IDF curves for return periods ranging from 5- to 100-year.

et al., 1988), which are often derived from univariate statistical analysis focusing on individual durations separately. Common design storms can be classified into four categories (Grimaldi & Serinaldi, 2006): (a) simple geometric patterns for which a single intensity-duration point is derived from the IDF curve (e.g., Chow et al., 1988); (b) temporal patterns adopting the entire IDF curve (e.g., Keifer & Chu, 1957, see e.g. the Chicago and Euler type II design storms in Figure 1); (c) standardized profiles derived from probabilistic analysis of observations (e.g., Huff, 1967); and (d) stochastically simulated patterns (e.g., Onof et al., 1996; Peleg et al., 2017). The choice of the type of design storm can have a significant impact on flood hazard estimation (Krvavica & Rubinic, 2020; Viglione & Blöschl, 2009).

Current limitations of design storms also arise from the approaches used for deriving their characteristics. This is illustrated in Figure 1, which compares observed precipitation events from Zurich (Switzerland, see details in Section 2) with the 100-year Chicago design storm (CDS) and Euler type II design storm that are constructed by adopting the entire IDF curve, that is, representing a precipitation event of a 100-year return level across all durations. It becomes clear from the visualization of the events in the IDF domain (Figure 1b) that adopting a single return period across all durations is a shortcoming for realistic construction of design storms, as it is highly unlikely for an extreme precipitation event that the precipitation volumes accumulated across different durations correspond to a single return-period. The CDS and Euler type II design storms can therefore be regarded as a worst-case scenario (Peleg et al., 2024), which do not account for the variability and corrected dependencies of the return periods across different durations within a storm.

Some studies have addressed the dependencies between precipitation across multiple durations through multivariate analysis. For example, Vandenberghe et al. (2010) presented a stochastic design storm generator that accounts for the joint probability of a design return period and a secondary return period, and Grimaldi and Serinaldi (2006) used a copula approach to estimate the joint probability of design precipitation volume (derived from the IDF curve), total precipitation, and peak intensity. In a similar analysis, Fontanazza et al. (2011) estimated the multivariate statistics of total precipitation, event duration, and peak intensity.

Here, we analyze multiple joint return period occurrences within precipitation events and develop a method to simulate design storms with parameterized sampling from the IDF curve. Specifically, we adopt a vine copula-based approach to estimate the co-occurrences of return periods over five different durations within a single precipitation event. We then generate precipitation time series that satisfy the observed duration-frequency statistics either by constraining a micro-canonical cascade model or by adopting the Euler Type II design storm profile construction guidelines. We demonstrate our methodology with data from Zurich (Switzerland) and provide readers with a simple, open-source model, for simulating design storms.

2. Data

Precipitation data at 10 min intervals were obtained from MeteoSwiss for the Zurich Affoltern, Fluntern, and Kloten stations (Figure S1 in Supporting Information S1) for the period 1981–2022. We assumed that the events from these stations occur independently yet belong to the same population as they experience a similar climate (Grimaldi & Serinaldi, 2006). Therefore, we pooled the data from all stations to increase the sample size of precipitation events representing Zurich, raising it from 42 years per station to a total of 126 years.

We defined independent events as wet periods separated by dry intermissions of at least 7 hr, following De Michele and Salvadori (2003), and applied the TENAX model (Marra et al., 2024) to compute the IDF curves for frequencies ranging from 1.1- to 100-year. The TENAX model relies on non-asymptotic statistics, which assumes that extremes are samples from the set of independent realizations of the process of interest. The IDF curves are hence obtained based on the cumulative distribution function of all events (also called "ordinary events") and not only from the annual maxima. For each event, we extracted the 360-min time series experiencing the maximum 360-min precipitation volume using a moving window and considered only these time series in the remainder of the study. This allows sampling events lasting 360 min or less. We then extracted the maximum 10-, 30-, 60-, and 180-min precipitation volumes from the 360-min long events. Lastly, we selected only those events reaching at least a 1.1-year return period, which is the minimum return level computed in the TENAX model, for one or more of the 10-, 30-, 60-, 180-, and 360-min durations. This results in a total of 537 events, which represents 3.5% of all 360-min events. This process allows to effectively sample the short-duration intense precipitation events in Zurich, as the time windows of the maximum 360-min precipitation volumes mostly coincide with the time windows in which the maximum 10-, 30-, 60-, and 180-min duration precipitation volumes occur (see Section 5).

3. Methodology

We propose a method for generating short-duration precipitation events based on the co-occurrence probabilities of multiple return periods over different durations within an event. The method relies on the dependence structure from the maximum 10-, 30-, 60-, and 180-min precipitation volumes within 360-min long observed events, and is estimated using a vine copula (Section 3.1). The vine copula can then be used to sample volumes over different durations within an event, thereby preserving the dependencies from the observed data. Next, we implement a constrained version of the bounded micro-canonical cascade model (Section 3.2) and of the Euler Type II design storm (Section 3.3) to generate precipitation time series that satisfy the copula-based volumes over different durations. We refer to the dependencies of the precipitation intensities over different duration intervals as the duration-frequency dependencies. Finally, we detail how precipitation time series can be generated based on the duration-frequency volume samples, exemplifying the methodology using data from Zurich (Section 4).

3.1. The Vine Copula

3.1.1. Pair-Copula Decomposition of the Multivariate Distribution

We model the multivariate relationship between the precipitation volumes on the 10-, 30-, 60-, 180- and 360-min intervals within our 537 events data set with copula. Let $\mathbf{X} = \{X_d\}$, where $d \in \{10, 30, 60, 180, 360\}$, represent the vector of precipitation volumes over the durations d. The multivariate probability distribution function F of $\mathbf{X}$ can be decomposed into its univariate marginal distributions $F_{d_1}, \ldots, F_{d_n}$ and a copula C that describes the dependence structure between the margins, according to Sklar's theorem (Nelsen, 2006; Sklar, 1959), with n equal to the number of intervals (durations), that is, five in our case study. The copula C is a joint cumulative distribution whose univariate marginal distributions $U_{d_1}, \ldots, U_{d_n}$ are uniform on [0, 1]. After estimating the univariate marginal distributions $u_d = F_d(X_d)$, the multivariate distribution $F(\mathbf{X})$ can be written as:

$$F(x_{10}, x_{30}, x_{60}, x_{180}, x_{360}) = C(u_{10}, u_{30}, u_{60}, u_{180}, u_{360}), \quad (1)$$

where the copula has the expression:

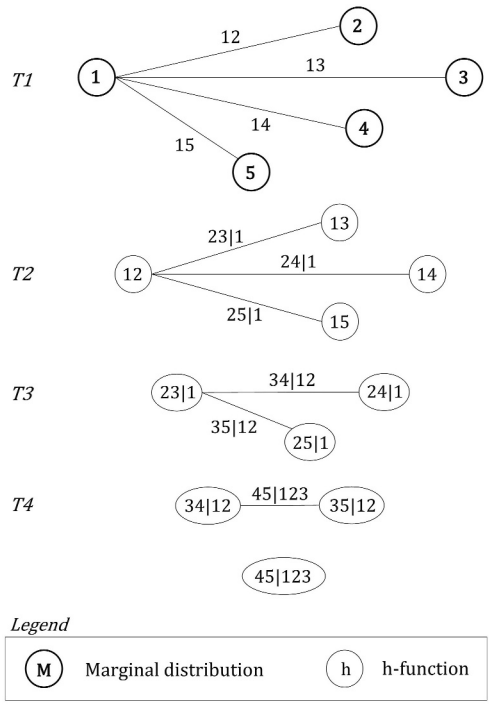

Figure 2. 5-Dimensional C-vine copula trees (*T1* to *T4*) with variable indexes i_d from 1 to 5.

$$C(u_{10},u_{30},u_{60},u_{180},u_{360}) = F\{F_{10}^{-1}(u_{10}),\ F_{30}^{-1}(u_{30}),\ F_{60}^{-1}(u_{60}),\ F_{180}^{-1}(u_{180}),\ F_{360}^{-1}(u_{360})\}. \quad (2)$$

For an absolutely continuous distribution F with strictly increasing continuous marginal densities, the joint density function f is obtained through the chain rule:

$$f(x_{d_1},\dots,x_{d_n}) = c_{d_1,\dots,d_n}\{F_{d_1}(x_{d_1}),\dots,F_{d_n}(x_{d_n})\}\cdot f_{d_1}(x_{d_1})\cdot\ \dots\ \cdot f_{d_n}(x_{d_n}). \quad (3)$$

Additionally, the joint density function can be factorized as

$$f(x_{d_1},\dots,x_{d_n}) = f_n(x_n)\cdot f(x_{n-1}|x_n)\cdot f(x_{n-2}|x_{n-1},x_n)\cdots f(x_1|x2,\ \dots\ ,x_n). \quad (4)$$

It follows from Equations 3 and 4 that we can construct the multivariate density iteratively as a product of pair-copulas.

For high-dimensional multivariate distributions, there are various possible pair-copula decompositions. The canonical vine copula (C-vine; Bedford & Cooke, 2002) is well suited to capture dependencies among variables when one variable exhibits dominant interaction within the data set. We defined X_{60} as the dominant variable as it exhibits the strongest pairwise dependencies with the volumes over the other durations (see Section 4). Hence, we adopted this type of copula tree construction, illustrated in Figure 2 and expressed as follows:

$$\begin{aligned} f(x_1,x_2,x_3,x_4,x_5) \ =\ & f_1(x_1)\cdot f_2(x_2)\cdot f_3(x_3)\cdot f_4(x_4)\cdot f_5(x_5) \\ & \cdot c_{12}\{F_1(x_1),F_2(x_2)\}\cdot c_{13}\{F_1(x_1),F_3(x_3)\} \\ & \cdot c_{14}\{F_1(x_1),F_4(x_4)\}\cdot c_{15}\{F_1(x_1),F_5(x_5)\} \\ & \cdot c_{23|1}\{F(x_2|x_1),F(x_3|x_1)\} \\ & \cdot c_{24|1}\{F(x_2|x_1),F(x_4|x_1)\}\cdot c_{25|1}\{F(x_2|x_1),F(x_5|x_1)\} \\ & \cdot c_{34|12}\{F(x_3|x_1,x_2),F(x_4|x_1,x_2)\}\cdot c_{35|12}\{F(x_3|x_1,x_2),F(x_5|x_1,x_2)\} \\ & \cdot c_{45|123}\{F(x_4|x_1,x_2,x_3),F(x_5|x_1,x_2,x_3)\}. \end{aligned} \quad (5)$$

The optimal structure, that is the ordering of the variables in $\mathbf{X} = \{X_d\}$, with $d \in \{10, 30, 60, 180, 360\}$, into the vector $\{X_i\}$, with $i \in \{1, 2, 3, 4, 5\}$, must be determined. The method used to determine the ordering is detailed hereafter.

3.1.2. Vine Copula Tree Structure

The structure of the C-vine copula is determined based on the dependencies between the variables (Nagler et al., 2017). These dependencies were estimated through the sum of the Kendall's τ rank correlation coefficient for each variable $\{X_d\}$:

$$\sum \tau_d = \sum_j (\tau_{j,d} \vee \tau_{d,j}), \quad (6)$$

where $\tau_{(d,j)} = \tau(X_d, X_j)$ and $d, j \in \{10, 30, 60, 180, 360\}$.

The C-vine structure index ordering i_d increases as the dependency of a variable within the data set decreases, that is the variable with the strongest dependencies within the data set has a variable index $i_d = 1$ and is located at the

root of the C-vine structure (Figure 2), while the variable with lowest dependencies within the data set has a variable index $i_d = 5$.

3.1.3. Non-Parametric Estimation of the C-Vine Copula

Once we established the optimal structure of the C-vine copula, we estimated the copula's parameters. Given that the margins of $\mathbf{X}$ are unknown, the estimation of the copula relies on the normalized ranks of the data, which serve as non-parametric estimates of the marginal distributions U_{10}, U_{30}, U_{60}, U_{180}, and U_{360}. Thereafter, the C-vine model is estimated following a procedure similar to the one described by Aas et al. (2009). This procedure involves a recursive estimation of bivariate conditional distributions, which are represented through the so-called h-function:

$$h(u|v) = P(U \leq u|V = v), \tag{7}$$

where U, $V \sim U[0, 1]$. For parametric models, such as the ones from the Archimedean and Elliptical copula families, the h-function can be readily obtained by estimating the derivative of the copula distribution function (Aas et al., 2009). This is possible because these types of copulas are expressed in terms of a parametric generator function.

Here, the variables in $\mathbf{X}$ exhibit asymmetric dependencies due to the following physical constraint:

$$\Pr_{d_1} \leq \Pr_{d_2} \quad \text{if} \quad d_1 \leq d_2, \tag{8}$$

where $\Pr_{d_1}$ is the cumulative precipitation volume in duration d_1. This leads to infeasible regions of the multivariate space, as it is visible in the lower right corner of the normalized rank data scatter plots shown later in Section 4. As a result, most families of parametric copulas, such as the Archimedean or Elliptical copulas that are designed to capture symmetric dependencies (Li et al., 2015), can not be used to model the variables in $\mathbf{X}$. While asymmetric parametric copulas can be constructed by combining families of symmetric copulas, the robustness of the copula model depends highly on the choice of the symmetric copula combinations and requires many parameters, potentially leading to over-parameterization (Y. Zhang et al., 2018).

The h-function was therefore estimated numerically. We adopted the adjusted Nadaraya-Watson conditional distribution estimator (Hall et al., 1999). The adjusted Nadaraya-Watson estimator of the h-function is defined as:

$$\hat{h}(u|v) = \frac{\sum_{i=1}^{n} \omega_i(v)\mathbb{I}(U_i \leq u)}{\sum_{i=1}^{n} \omega_i(v)}, \tag{9}$$

where

$$\omega_i(v) = p_i(v)K_{b_n}(v - V_i)\sum_{j=1}^{n} p_j(v)(v - V_j)^2 K_{b_n}(v - V_i), \tag{10}$$

and

$$K_{b_n}(\cdot) = \frac{K\left(\frac{\cdot}{b_n}\right)}{b_n}, \tag{11}$$

with K being a kernel function. $b_n > 0$ is a bandwidth, and $\mathbb{I}$ is the indicator function such that

$$\mathbb{I} = \begin{cases} 1 & \text{if } U_i \leq u \\ 0 & \text{if } U_i > u \end{cases}, \tag{12}$$

and

$$p_i(v) = \frac{1}{n} \cdot \frac{1}{1 + \lambda(v)(v - V_i)\, K_{b_n}(v - V_i)}. \tag{13}$$

$\lambda(v)$ solves the equation:

$$\sum_{i=1}^{n} p_i(v)(V_i - v)\, K_{b_n}(V_i - v) = 0, \tag{14}$$

which can be estimated numerically using the Newton-Raphson algorithm, with the bandwidth $b_n = n^{-1/3}$ and the Gaussian kernel function K given by $K(x) = \frac{e^{-0.5x^2}}{\sqrt{2\pi}}$.

3.1.4. Sampling From the C-Vine Copula

We followed the algorithm presented in Aas et al. (2009) to simulate the N samples from the C-vine copula, where N is the sample size. In this algorithm, sampling dependent uniform variables from a C-vine copula is achieved by modeling a cascade of pair-copula, consisting of repeated use of the fitted h-functions. The resulting sample contains the simulated dependent uniform variables $\tilde{u}_d$. Ultimately, the simulated sample of the random variables $\widetilde{\mathbf{X}}$ is estimated using the inverse of the empirical or fitted marginal cumulative distribution functions.

While the numerical estimation of the h-function captures the asymmetric dependencies to a very good approximation, it does not enforce a strict boundary for the physically infeasible region of the multivariate space. That is, some sampled variables could violate the physical constraint in Equation 8, thereby generating unrealistic precipitation intensities across durations. To address this, we apply the following correction to the variables $\widetilde{\mathbf{X}}$, ensuring that the corrected precipitation volumes $\widetilde{\mathbf{X}'}$ are at least as large on the interval $d + 1$ as on the interval d:

$$\widetilde{X'}_d = \begin{cases} \tilde{X}_d, & \text{if } d = 10 \\ \max\{\widetilde{X'}_{d-1}, \tilde{X}_d\}, & \text{if } d \in \{30, 60, 180, 360\} \end{cases}. \tag{15}$$

Uncertainties in the modeling of the C-vine copula are estimated by repeated sampling of the fitted model, similar to the procedure outlined in Ribeiro et al. (2020). We simulate 10,000 realizations of extreme precipitation intensities, each with a sample size equal to the original data set, that is 537. The 99% confidence intervals of Kendall's τ rank correlations of the simulated samples are compared with the correlations of the observed data pairs, thereby estimating the uncertainties associated with the conditional probabilities and verifying that the simulated samples maintain the dependencies in the observations.

3.1.5. Conditional Sampling From the C-Vine Copula

The algorithm presented in Aas et al. (2009) can also be applied to simulate N samples from the C-vine copula with a fixed return period over one of the duration intervals. In this case, the precipitation volume corresponding to the required return period over this duration interval is first identified. The uniform variable u_d associated with the fixed precipitation volume is estimated using the marginal cumulative distribution function. The uniform variables on the other duration intervals are then computed based on the fixed uniform variable and following the algorithm outlined in Aas et al. (2009). Similar to the non-conditional sampling from the C-vine copula, the simulated sample of the random variables $\widetilde{\mathbf{X}}$ is then estimated using the inverse of the empirical or fitted marginal cumulative distribution functions, and corrected following Equation 15.

3.2. Constrained Micro-Canonical Cascade Model

After simulating the precipitation intensities over different durations using the C-vine copula, precipitation time series were constructed using a constrained bounded micro-canonical cascade model, which ensures that the profiles align with the properties of the duration-volume samples. This model builds on the micro-canonical cascade model introduced by Olsson (1998), which disaggregates precipitation amounts from a coarse time step into finer time steps and preserves the precipitation amount exactly throughout the disaggregation process. The precipitation in disaggregation level l is subdivided into b finer time steps in the disaggregation level $l + 1$,

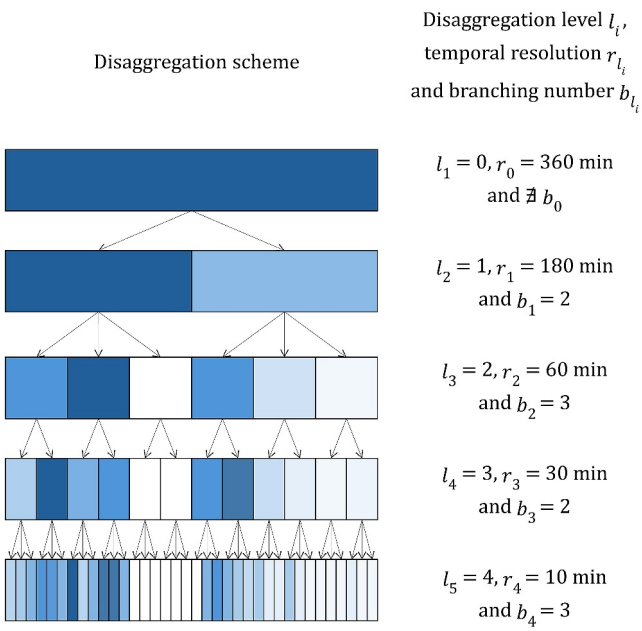

Figure 3. Disaggregation scheme of the constrained bounded micro-canonical cascade model. The dark blue color (as in the box of disaggregation level l_1) indicates the location of the constraining volumes in each of the levels and lighter colors indicate smaller volumes, relative to the constraining volume of each level. In the illustrated example, the constraining volumes are $V_0 = 34$ mm, $V_1 = 20.5$ mm, $V_2 = 11.3$ mm, $V_3 = 6.1$ mm, and $V_4 = 2.5$ mm.

where b is the branching number. Micro-canonical cascade models are frequently used to temporally downscale precipitation time series for hydrological applications (e.g., Güntner et al., 2001; Müller & Haberlandt, 2018; Müller-Thomy, 2020). Here, we further develop the model and introduce constraints derived from the duration-volume samples, whose validation is presented in Figure S2 of Supporting Information S1.

3.2.1. The Branching Structure

The branching structure of the constrained bounded micro-canonical cascade model is presented in Figure 3. Depending on the disaggregation level l_i, the branching number takes values $b = 2$ or $b = 3$. Starting with a 360-min temporal resolution, the precipitation volume is successively subdivided into smaller time increments of 180-, 60-, 30-, and 10-min intervals. The $b = 3$ splitting is required to achieve a final temporal resolution of 10 min. It was implemented from temporal resolutions of 180 min to 60 min and from 30 min to 10 min. This allows the inclusion of intermediate temporal resolutions that are commonly used for design purposes. During this disaggregation process, precipitation is split according to weights W, which determine the fraction of precipitation amount in the branches departing from a wet cell.

For branching number $b = 2$, the cascade model can have one of three states, each associated with a specific probability of occurrence:

$$W_1, W_2 = \begin{cases} 1, 0 & \text{with probability } P(1,0) \\ 0, 1 & \text{with probability } P(0,1) \\ x, 1-x & \text{with probability } P(x, 1-x) \end{cases}, \tag{16}$$

where W_1 and W_2 are the weights of the first and second branches respectively, and x is the relative fraction of the precipitation volume that is assigned to the first of the two finer time steps when both finer time steps are wet. The variable x is a random variable from a known probability distribution, with $x \in [0, 1]$.

For branching number $b = 3$, the cascade model can assume one of seven states, each associated with a specific probability of occurrence:

$$W_1, W_2, W_3 = \begin{cases} 1, 0, 0 & \text{with probability } P(1,0,0) \\ 0, 1, 0 & \text{with probability } P(0,1,0) \\ 0, 0, 1 & \text{with probability } P(0,0,1) \\ x, 1-x, 0 & \text{with probability } P(x, 1-x, 0) \\ x, 0, 1-x & \text{with probability } P(x, 0, 1-x) \\ 0, x, 1-x & \text{with probability } P(0, x, 1-x) \\ x, y, 1-x-y & \text{with probability } P(x, y, 1-x-y) \end{cases}, \tag{17}$$

where W_1, W_2 and W_3 are the weights of the first, second, and third branches respectively, x is the relative fraction of the precipitation volume that is assigned to the first of the finer time steps that is wet, and y is the relative fraction of the precipitation volume that is assigned to the second finer time steps when all finer time steps are wet. The variable x is a random variable from a probability distribution and the variable y is a random variable from a probability distribution of y conditioned on x, with $x, y \in [0, 1]$.

The parameters of the cascade model are hence the probabilities of occurrence of the possible states and the distributions of x and y. The parameters can be estimated by aggregating observed time series to the temporal resolutions of the model. Here, a bounded cascade model is applied, in which the weights W depend on the

disaggregation level. This allows the disaggregation process to become smoother with finer resolutions, and to capture the different underlying processes across the range of temporal resolutions (Müller-Thomy, 2020).

The empirical probability distributions of x are estimated separately for each disaggregation level using 14 equidistant bins (Müller-Thomy, 2020). When $b = 3$, the empirical probability distributions of y are obtained by binning the histograms of x into 7 equidistant intervals and estimating the empirical probability distribution of y using 14 equidistant bins (Lisniak et al., 2013).

3.2.2. Constraining the Micro-Canonical Cascade Model

The model is further developed to accommodate constraints from the duration-volume samples obtained from the vine copula. These samples contain the 10-, 30-, 60-, 180- and 360-min maximum precipitation volumes of the design storm. Thus, the bounded micro-canonical cascade model must be constrained such that the sampled volumes occur at least once in each of the respective temporal resolutions. Hereafter, we will refer to the sampled volumes as the "constraining volumes", and to the process as "constraining the model." By introducing these constraints, this model is not fully stochastic anymore, similar to the model described in Müller-Thomy (2020).

Constraining the lowest disaggregation level l_1 is straightforward, as we simply assign the precipitation volume sampled for the 360-min duration to this level. For the higher disaggregation levels, we must first determine the temporal location of the constraining volume. To do so, we distinguish between two cases; either the constraining volumes are aligned between subsequent disaggregation levels, or they are not aligned. We consider constraining volumes to be aligned if the constraining volume in level l_{i+1} arises from the subdivision of the constraining volume in level l_i. This is illustrated in Figure 3, where constraining volumes are aligned if they are connected by an arrow between subsequent disaggregation levels (in the example from Figure 3, the constraining volumes are thus aligned between disaggregation levels l_1 and l_2, as well as between l_2 and l_3, but not between l_3 and l_4, or between l_4 and l_5).

To determine whether the constraining volumes are aligned, we must first verify that the non-constraining volumes allow misalignment, that is, that at least one non-constraining volume in level l_i is higher than the constraining volume in l_{i+1}:

$$M_{i+1} = \sum \mathbb{I}\left(V^*_{l_i} > V_{l_{i+1}}\right)$$

$V^*_{l_i}$ are the non-constraining volumes of disaggregation level l_i and $V_{l_{i+1}}$ is the constraining volume of the level l_{i+1}. If $M_{i+1} = 0$, the constraining volumes cannot be misaligned, and therefore the constraining volume in level l_{i+1} must arise from the subdivision of the constraining volume in level l_i. If $M_{i+1} = 1$, additional parameters associated with the positioning of the constraining volume in level l_{i+1} are introduced. These parameters describe the probabilities of the constraining volume $V_{l_{i+1}}$ to be in any of the time steps in this level. Similarly to the parameters of the bounded micro-canonical cascade model, these parameters can be estimated by aggregating the observed time series from the 537 events data set to the temporal resolutions of the model.

Here, the constraining volume positioning probabilities are estimated depending on the disaggregation level as well as the position of the constraining volume in the previous disaggregation level. In the example from Figure 3, $M_4 = 1$ and the position probabilities for level l_4 given that the V_{l_3} occurs in the second time step of level l_3 are: $P_{\text{pos}} = \{0.01, 0.28, 0.31, 0.33, 0.05, 0, 0, 0, 0, 0, 0.01, 0.01\}$. Hence, the probability of the constraining volume V_{l_4} to occur in the second time step of level l_4, as shown in Figure 3, is 28%.

In either case, whether $M_{i+1} = 0$ or $M_{i+1} = 1$, and once the position of $V_{l_{i+1}}$ is known, the volume at level l_i that generates the constraining volume $V_{l_{i+1}}$ can be identified, and the volumes in all time steps of level l_{i+1} can be estimated. First, the volume at level l_i that generates the constraining volume $V_{l_{i+1}}$ is subdivided. The state that the model assumes is estimated depending on the relationship between V_{l_i} and $V_{l_{i+1}}$. If $V_{l_i} > V_{l_{i+1}}$, the following states are not possible: {1,0} and {0,1} for $b = 2$, and {1, 0, 0}, {0, 1, 0} and {0, 0, 1} for $b = 3$. In that case, the relative fractions of volume assigned to the finer time steps are sampled from their empirical probability distributions. If $M_{i+1} = 0$, the constraining volume $V_{l_{i+1}}$ is assigned to any of the highest fractions, and if $M_{i+1} = 1$, the position of $V_{l_{i+1}}$ is already known. For $b = 2$, or if $b = 3$ and one of the finer time steps is dry, the fraction of volume in the other wet time step is simply $1 - V_{l_{i+1}}/V_{l_i}$. For $b = 3$ and all finer time steps are wet, the fraction y is sampled

depending on $x = V_{l_{i+1}}/V_{l_i}$. If $V_{l_{i+1}} = V_{l_i}$, either $M_{i+1} = 0$, in which case we generate states until the weights are a combination of 0 and 1, or $M_{i+1} = 1$ and the position of $V_{l_{i+1}}$ is already known. Second, the volumes at level l_i that do not generate the constraining volume $V_{l_{i+1}}$ are subdivided. This is done similarly to the bounded micro-canonical cascade model, except that no precipitation volume can exceed the constraining volume.

Lastly, the maximum 10-, 30-, 60-, and 180-min precipitation volumes are computed using a moving window with a step size of 1. This operation is necessary to ensure that the maximum precipitation volumes over the different duration intervals do not exceed the constraining volume. In the micro-canonical cascade model, the precipitation volumes from a coarse time step can be regarded as the moving window sum of the finer time step, with the moving window size and step size equal to the branching number. In the disaggregation scheme from Figure 3 and for a disaggregated precipitation event, the precipitation volumes at level l_4 can hence be computed by summing the precipitation volumes at level l_5 by using a moving window with a window size of 3 and a step size 3. Therefore, the actual maximum precipitation volumes over the different duration intervals must be computed with a moving window with a window size of 3 and a step size 1. If this operation results in maximum precipitation volumes that exceed the constraining volumes, the disaggregation of the event is disregarded and repeated.

3.3. Euler Type II Design Storm Profiles

For comparison with design storm profiles used in engineering applications, we also implement the simulation of an Euler Type II design storm profile based on the duration-frequency samples from the vine copula. This type of design storm is commonly used in several European countries for the planning of infrastructure. It is usually constructed by following the entire IDF curve for a certain frequency (Figure 1). We will refer to the Euler Type II design storm following the entire IDF curve as a "standard Euler Type II design storm", and to the design storms based on the duration-frequency samples from the vine copula as "constrained Euler Type II design storms" hereafter. Both design storms are similarly constructed, that is by sorting the precipitation intensities from the largest to the smallest value and flipping the first one-third of the sorted data (DWA-A 118, 2006).

4. Case Study: Simulating Realistic Design Storms for the City of Zurich

4.1. Duration-Frequency Dependencies

The structure of the C-vine copula is first analyzed. In the observed precipitation data in Zurich, the 60-min interval precipitation volume exhibits the strongest pairwise dependencies with the other duration intervals, as it has the highest $\sum\tau_d$ (Figure 4). The pairwise dependencies for the other durations decrease in the following order: 30-, 180-, 10-, and finally 360-min intervals. The variable indexes of the C-vine copula are thus $i_{10} = 4$, $i_{30} = 2$, $i_{60} = 1$, $i_{180} = 3$, and $i_{360} = 5$.

Once the structure of the C-vine copula is determined, the h-functions are estimated, and the C-vine copula is then constructed. Numerical estimations of the h-functions are shown in Figure S3 of Supporting Information S1.

4.1.1. Simulating Precipitation Intensities Over Different Durations Through Random Copula Sampling

The samples simulated from the C-vine copula effectively capture the dependencies (Figure S4 in Supporting Information S1), with envelopes of simulated samples similar to the ones of ranked observed data. Additionally, the bivariate dependencies, as measured by Kendall's τ rank correlation coefficients, are overall well reproduced by the C-vine copula, with a mean absolute difference of 0.05. However, a few samples are beyond the physical boundaries defined in Equation 8. This is rectified after applying the adjustment introduced in Equation 15, as shown in Figure 4. After correction, the envelopes of simulated samples are similar to the ones of ranked observed data and respect the boundaries of the physically infeasible region in the lower right corner of the scatter plots. The bivariate dependencies slightly increase due to the correction, as the latter forces physically unfeasible samples toward the secondary diagonal. Consequently, the histograms of simulated Kendall's τ rank correlation coefficients related to the 180- and 360-min volumes shift from being equal or lower than the observed Kendall's τ in Figure S4 of Supporting Information S1 to being greater in Figure 4. The mean absolute difference between the observed Kendall's τ and that of the corrected simulated samples is 0.06, with observed Kendall's τ rank correlation coefficients falling outside of the 99% confidence intervals of τ from corrected simulated samples for the pairs of 30- and 60-min, 10- and 180-min, 10- and 360-min, 30- and 360-min, and 60- and 360-min. Nevertheless,

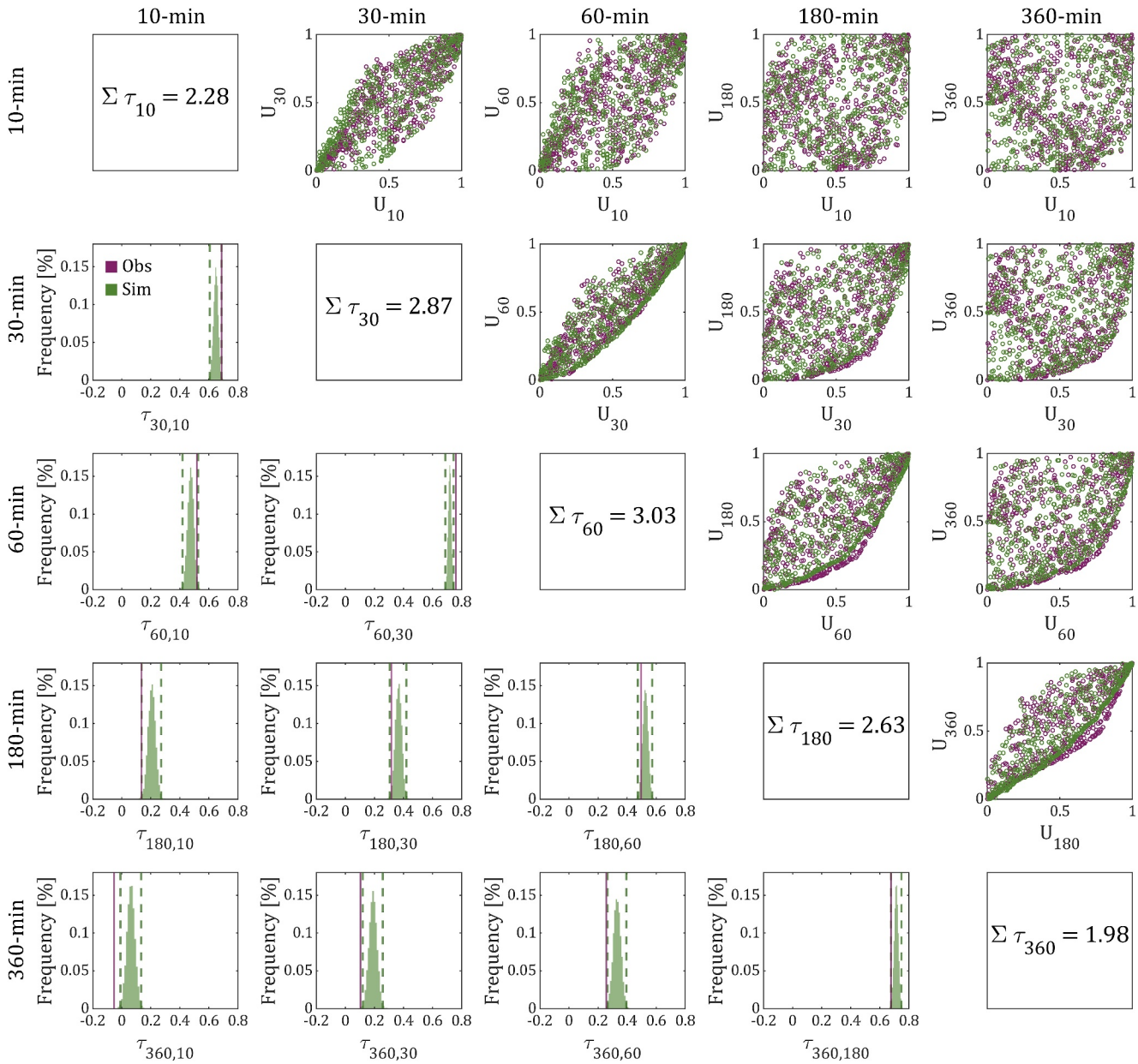

Figure 4. Above the diagonal: scatter plots of the precipitation volumes on the 10-, 30-, 60-, 180-, and 360-min duration intervals within one precipitation event, comparing simulated samples after adjustment through Equation 15 (green) with the ranked observations (purple), both with a sample size of 537. Below the diagonal: histograms of the pairwise Kendall's τ rank correlations based on 10,000 simulations, each with a sample size of 537. The 99% confidence interval bounds are shown by dashed lines and the τ rank correlations of the observations are shown by the vertical purple lines. Along the diagonal: estimates of the observed pairwise dependencies of each duration interval with the other duration intervals, following Equation 6.

the bounds of the 99% confidence intervals are close to the observed Kendall's τ rank correlation coefficients. The absolute differences between the nearest 99% confidence bound of τ from the corrected simulated samples and τ of observed data are 0.01, 0.00, 0.04, 0.01, and 0.01, respectively. We will refer to the corrected simulated samples simply as simulated samples hereafter.

The simulated precipitation volumes are then derived from the uniform variables $\tilde{u}_d$ and the inverse of the marginal distributions of $\mathbf{X}$. Since the marginal distributions are not known, we fitted the Gamma and Lognormal distributions. On average, the Gamma distribution yields a 1.5% higher loglikelihood than the Lognormal distributions. However, for higher precipitation volumes (above the 90th percentile), the Lognormal distribution provides a better fit, with a loglikelihood on average 1.9% higher than that of the Gamma distribution.

10.1029/2024WR039739

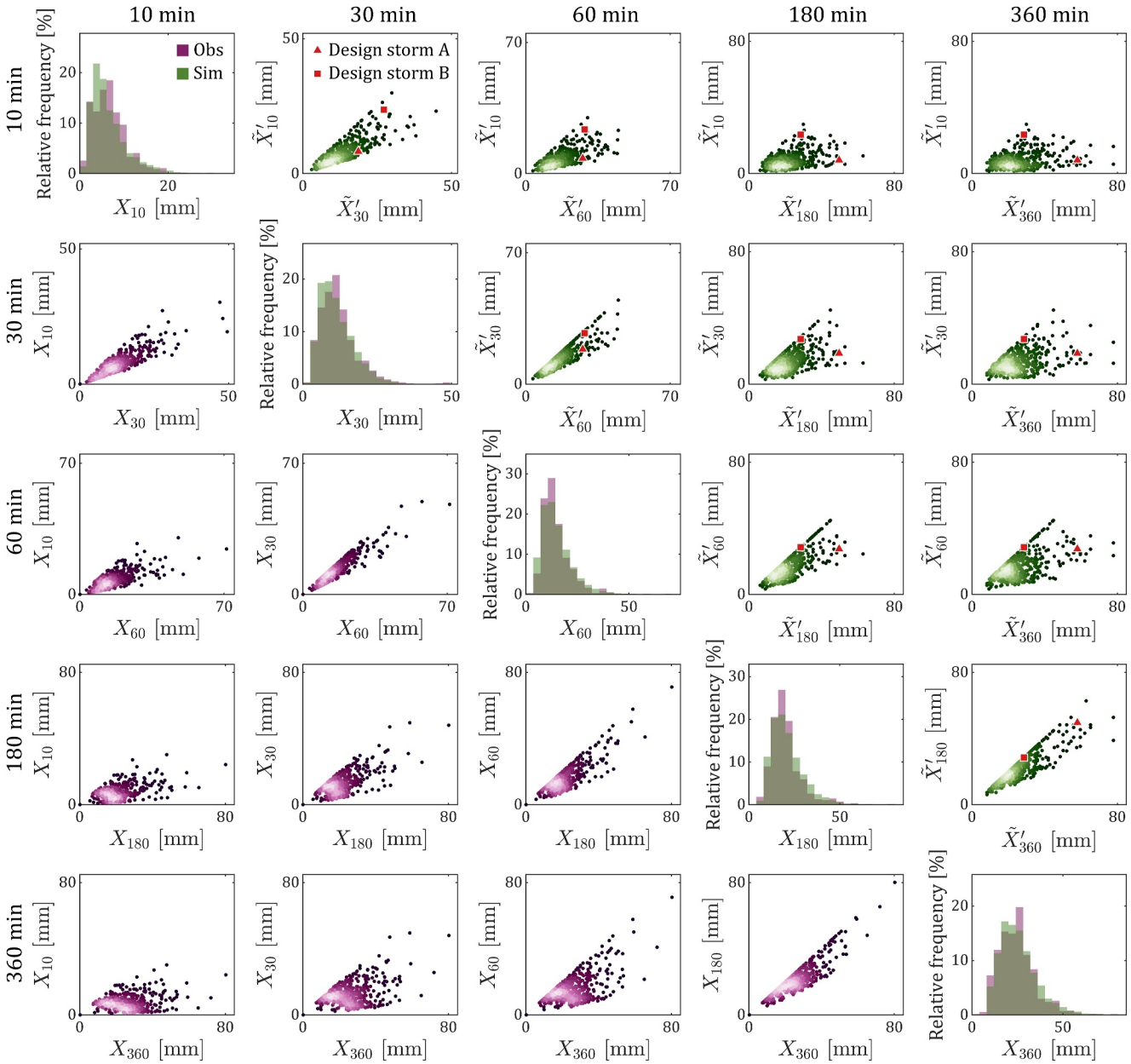

Figure 5. Below and above the diagonal: scatter plots of observed (purple) and simulated (green) precipitation volumes. The simulated samples correspond to one simulation with a sample size of 537. Lighter color shadings represent a higher density of the data. The red triangle and the red square indicate the precipitation volumes used to derive the design storms labeled A and B in Figure 7. Along the diagonal: histograms of observed (purple) and simulated (green) precipitation volumes. The simulated samples correspond to 10,000 simulations, each with a sample size of 537.

Considering that the higher precipitation volumes are the most critical ones for design storms, and that both distributions achieve a good fit across the full range of precipitation volumes, we used the Lognormal distribution to fit the margins. As discussed in Section 5, we regard the choice of distribution as a parameter, and the model offers users the flexibility to select different statistical distributions in regions or for durations with distinct precipitation distributions. The fitted density functions and cumulative probability functions are shown in Figure S5 of Supporting Information S1. Figure 5 displays the simulated precipitation volumes $\widetilde{\mathbf{X}'}$ corresponding to the sampled uniform variables shown in the scatter plots in Figure 4. The fitted marginal distributions effectively reproduce both the frequently occurring volumes and the extreme values, matching the distribution of the observed data (Figure S5 in Supporting Information S1).

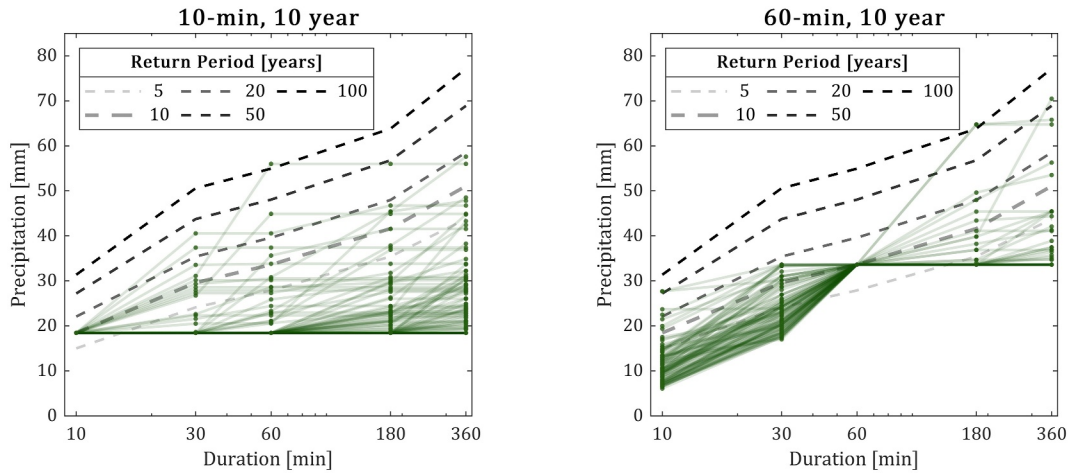

Figure 6. Copula samples for given duration-frequency conditions: 10-year return period for the 10-min duration interval (left), and 10-year return period for the 60-min duration interval (right). Sample sizes are 100. Darker colors indicate overlapping lines.

4.1.2. Simulating Precipitation Intensities Over Different Durations Through Conditional Copula Sampling

We have demonstrated that we can simulate precipitation intensities over different durations, based on random sampling from the C-vine copula. The simulated precipitation intensities thereby satisfy the duration-frequency dependencies of observed events (Figures 4 and 5). Another functionality of the model is to simulate precipitation intensities over different durations, based on conditional sampling from the C-vine copula. We present 100 random copula samples that meet specific conditions in Figure 6, pivoting on precipitation volumes over the 10- and 60-min duration intervals for the 10-year return period (and over the 360-min interval in Figure S6 of Supporting Information S1). This is achieved by carrying conditional sampling from the vine copula, conditioned on user-defined precipitation volume over a duration interval (here over the 10-min and 60-min intervals respectively in Figures 6, and 360-min interval in Figure S6 of Supporting Information S1). Duration-frequency profiles of observed events with similar characteristics are shown in Figure S7 of Supporting Information S1. The simulated events present a variety of duration-frequency profiles, similar to observed events. This variability results in large confidence intervals, defined as the range between the 1st to 99th percentile, of the relative difference of total storm volume between design storms adopting the entire IDF curve and 10,000 simulated design storms following the presented methodology (Table 1). Most events have lower return periods on duration intervals longer than the one from the duration-frequency condition, that is on duration intervals longer than 10- and 60-min, respectively (Figure 6). However, some events have higher return periods on longer duration intervals, reaching up to 100-year return periods in both cases. This translates to the negative values of the first

Table 1
Mean (μ, in Bold in the Table), First Percentile (q_1) and 99th Percentile (q_{99}) of the Relative Difference (in %) of Total Storm Volume Between Design Storms Adopting the Entire IDF Curve (Such as the CDS or the Standard Euler Type II Design Storm, for Example) and 10′000 Design Storms Following the Presented Methodology, for Different Duration-Frequency Conditions (Following Similar Conditioning as in Figure 6)

	5-year			10-year			20-year			50-year			100-year		
	q_1	μ	q_{99}	q_1	μ	q_{99}	q_1	μ	q_{99}	q_1	μ	q_{99}	q_1	μ	q_{99}
10 min	−32	**42**	66	−13	**48**	62	−2	**52**	62	16	**56**	61	23	**56**	59
30 min	−36	**31**	45	−22	**34**	42	−7	**35**	39	7	**35**	36	15	**34**	34
60 min	−42	**26**	36	−22	**30**	34	−2	**31**	32	16	**30**	30	20	**29**	29
180 min	−32	**16**	19	−17	**17**	18	−6	**17**	18	5	**17**	18	15	**17**	17
360 min	0	**0**	0	0	**0**	0	0	**0**	0	0	**0**	0	0	**0**	0

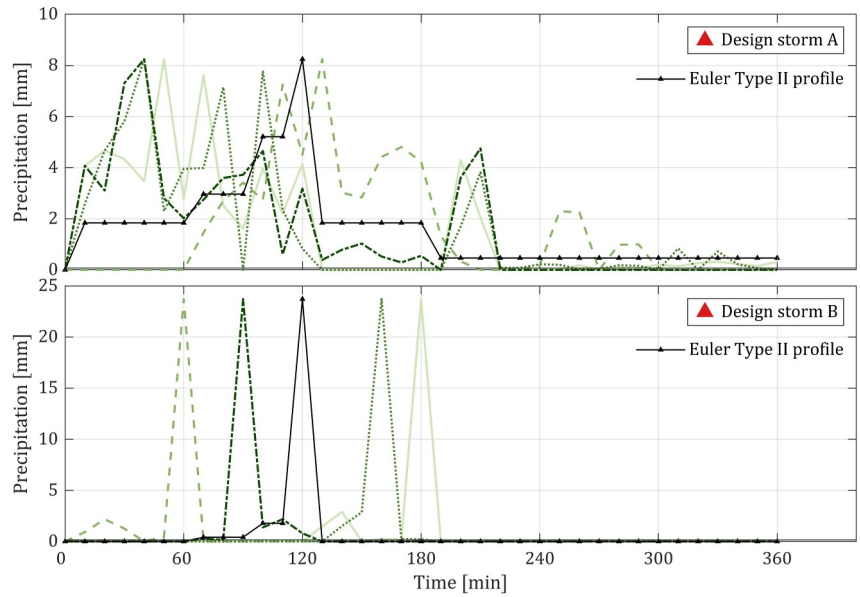

Figure 7. Precipitation hyetographs generated using the precipitation volumes for design storms A and B presented in Figure 5. The green lines show the profiles constructed using the constrained bounded micro-canonical cascade model and the black lines show the profiles constructed using the Euler Type II design storm guidelines.

percentile of the relative difference in total storm volumes in Table 1. Importantly, contrary to the CDS or standard Euler Type II design storms, none of the duration-frequency profiles follow a single frequency on all duration intervals (Figure 6, Figures S6 and S7 in Supporting Information S1). As a result, the 10-year storms over a 10-min or over a 60-min duration interval, as presented in Figure 6, have an average reduction in total storm volume of 48% and 30% respectively (Table 1) compared to design storms following the entire IDF curve (such as in the CDS or standard Euler type II design storm approach). The relative difference in total storm volume between design storms adopting the entire IDF curve and design storm from conditional vine copula samples is largest for conditional return period of 50 years (Table 1). We can also notice that the relative difference in total storm volume decreases when the conditional sampling is applied to longer duration intervals. This is expected as the total storm volume is approximated by the storm volume on the 360-min duration interval and that the pairwise dependencies are largest for consecutive duration intervals than for non-consecutive ones (Figure 3). Therefore, as the pivoting condition is applied to durations closer to the 360-min interval, its influence on the total storm volume increases. The confidence intervals in Table 1 are further discussed in Section 5.

4.2. Design Storm Profiles Simulation

4.2.1. Simulating Design Storms With the Constrained Micro-Canonical Cascade Model

Precipitation time series simulated using the constrained micro-canonical cascade model are based on the copula-simulated precipitation volumes. The constrained bounded micro-canonical cascade model can generate multiple profiles of design storms for a single duration-frequency data set. Figure 7 showcases randomly generated profiles for two samples simulated by the copula; one with distributed precipitation volumes throughout the design storm (design storm A) and another with an intense 10-min burst (design storm B). The constraints applied to the cascade model for design storm B result in similar profiles, whereas the constraints for design storm A allow for greater flexibility, producing more varied shapes.

We validated the coupled vine-copula and constrained bounded micro-canonical cascade model by analyzing the timing of peak volume, intermittency duration, and number of intermittencies within an event (Figure 8). Here, intermittencies refer to dry spells, without any constraint of being bracketed by wet spells. We compared these properties from the observed events with the ones from 10,000 precipitation profiles generated for each of the 537 copula samples shown in Figure 5. Simulated and observed precipitation profiles are front-loaded (i.e., a greater percentage of precipitation falls early in the event), with the 10-min peak occurring within the first hour of the

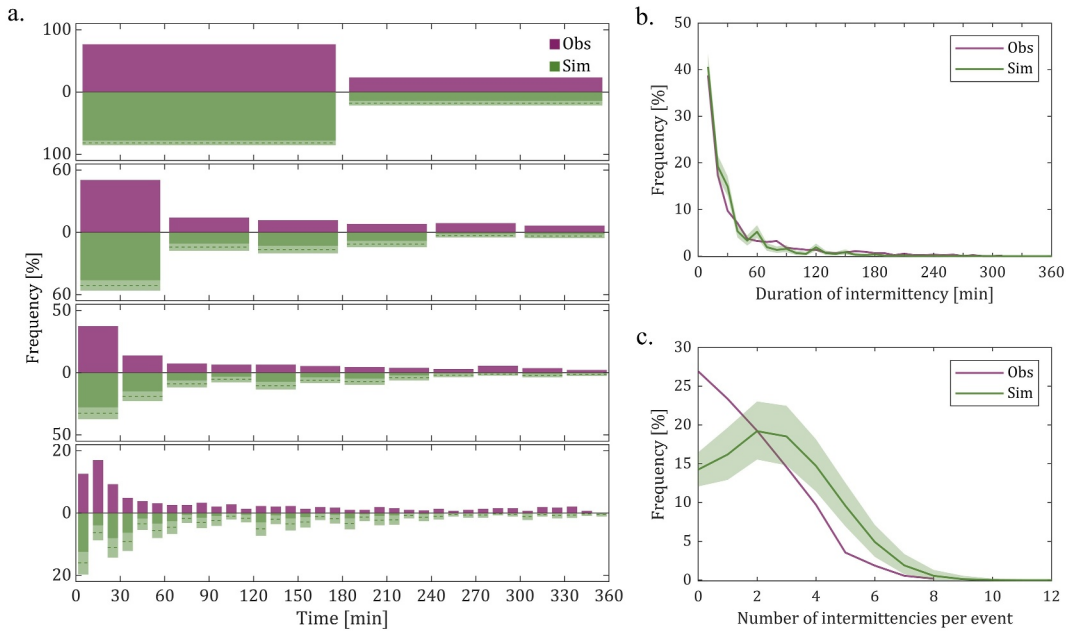

Figure 8. Validation of the coupled vine-copula and constrained bounded micro-canonical cascade model. Simulated events are generated using the constraining volumes from the randomly copula-sampled events. We generated 10,000 simulations, each with a sample size of 537. (a) Histogram of peak volume location across disaggregation levels for simulated events (green) and aggregated observed events (purple). Temporal resolutions of the disaggregation and aggregation levels correspond to the width of the boxes (from top to bottom: from 180- to 10-min). Shaded green boxes represent the 1st to 99th percentile bounds of the 10,000 simulated data sets, and dotted green lines indicate the mean values. (b) Frequency of intermittency durations within events. (c) Frequency of intermittency counts per event. In (b, c), shaded areas represent the 1st to 99th percentile bounds over the 10,000 simulated data sets, and the bold line indicates the mean value.

hyetograph in 53.6% of the observed events and, on average, in 51.2% of the simulated events (Figure 8a). The constrained micro-canonical cascade model slightly underestimates the occurrence of back-loaded events, with the 10-min peak occurring within the second half of the event in 23.3% of observed events and, on average, in 18.0% of simulated events. Most intermittencies are short in both observed and simulated events, with intermittencies lasting for only 10-min in 40.8% of the observed events and, on average, in 38.8% of the simulated events (Figure 8b). Overall, the durations of the intermittencies are well captured by the constrained micro-canonical cascade model. The number of intermittencies per event is overestimated in the simulated events, with on average 14.3% of simulated events showing no intermittency, while this proportion rises to 26.9% for observed events (Figure 8c). Less than 1% of events have more than 9 intermittencies in the simulated and observed events.

4.2.2. Simulating Constrained Euler Type II Design Storms

We also simulated the precipitation time series following the Euler Type II design storm construction guidelines, using the randomly sampled precipitation volumes on the 10-, 30-, 60-, 180-, and 360-min intervals. In this case, only one precipitation profile can be generated per duration-frequency sample, unlike the constrained micro-canonical cascade model, which allows multiple realizations. Figure 7 showcases the constrained Euler Type II design storms for design storms A and B. For design storm A, with distributed precipitation volumes throughout the design storm, the constrained Euler Type II design storm profile varies significantly from the ones generated by the constrained micro-canonical cascade model. Notably, the constrained Euler Type II design storm displays no intermittency. For design storm B however, there is a high resemblance between the profiles generated using the cascade model and the one following the Euler Type II design storm guidelines. This is due to the characteristics of the constraining volumes, enforcing an intense 10-min burst and almost no precipitation on the remainder of the time series.

5. Discussion

We propose a new method for generating design storms based on the co-occurrence probabilities of multiple return periods over different durations within a single precipitation event. The method is overall able to reproduce the duration-frequency dependencies within short-duration precipitation events (Figures 4 and 5), and to satisfy the physical constraint of Equation 8, thereby addressing the unrealistic sampling from parametric copula (Grimaldi & Serinaldi, 2006). This is achieved through the use of non-parametric copulas that can capture the observed asymmetric dependencies arising from the fact that precipitation volumes on lower duration intervals can not exceed those from longer duration intervals (Figure S4 in Supporting Information S1), and through the correction from Equation 15. Unlike the current applications of most design storms, the method explicitly accounts for the range of possible return period co-occurrences over different durations. Additionally, a key aim of the study was to propose a reproducible and usable method for stakeholders, as highlighted in Wright et al. (2021). As such, the micro-canonical cascade model was chosen for deriving the precipitation time series not only due to its ability to conserve precipitation volume throughout the disaggregation process but also for its simplicity, its ease of parametrization, and the ease of application of the constraining volumes across different durations. The model is fast as it takes less than 0.01 s using a regular computer to generate a storm using the proposed coupled vine copula and constrained micro-canonical cascade model. We also propose the Euler Type II design storm profile as an alternative to the micro-canonical cascade model. Although this type of design storm does not reproduce the characteristics of the observed events, mainly in terms of intermittency, it follows engineering guidelines used in various European countries.

We use the 10-, 30- 60-, 180-, and 360-min intervals as these durations are commonly used to analyze convective precipitation events (Derx et al., 2023; Fowler et al., 2021; Peleg et al., 2024; Villalobos Herrera et al., 2024). They effectively capture the dynamics of the entire 6-hr precipitation profile by covering various durations throughout the storm and cover a period during which the majority of intense short-duration precipitation events occur (Huff, 1975; Visser et al., 2023). Additionally, the time of concentration is typically used to determine the total duration of the design storm in urban drainage design as it ensures that the design storm is long enough for the precipitation from the whole catchment to contribute to the flow in the system (Grimaldi & Serinaldi, 2006; Keifer & Chu, 1957), and this time is typically shorter than 6 hr for urban catchments (Arnbjerg-Nielsen et al., 2013; Chow et al., 1988). Furthermore, the selected durations allow straightforward application of the micro-canonical cascade model with branching $b = 2$ and $b = 3$. Nevertheless, the presented methodology allows for a flexible number of duration intervals and could also be applied for different duration intervals, namely if observed data are available at different temporal resolutions or if the time of concentration is longer than 6 hr. However, the dependencies between durations approach zero as the duration difference increases, with a rank correlation close to zero for the 360- and 10-min duration intervals (Figure 4). Thus, using duration intervals that have large differences, and possibly represent extremes from different storm types (e.g., 1 hr for convective storms and 48 hr for large synoptic-scale storms), is unlikely to yield additional information with respect to a standard univariate approach.

We analyze the effect of the observation data sample size in Figure S8 of Supporting Information S1, by comparing the IDF curves of samples representing 20-year to 124-year of data, obtained from bootstrapping of the observed data. The 1st to 99th percentile confidence interval of the IDF curves remains almost constant for observation data sample sizes from 40- to 124-year. Thus, the three climate stations from Zurich independently maintain this data (42 years of observations) without requiring pooling. The analysis of record length implies that, for applications using similar temporal scales as in this study, single climate stations may possess sufficient information to extract the IDF curves. Furthermore, our data sample consists of 537 events, which is larger than the ones from studies using similar copula-based approaches to evaluate the joint probability of precipitation characteristics in sub-daily events (e.g., Fontanazza et al. (2011) and Grimaldi and Serinaldi (2006) used 144 and 70 events, respectively). The model is inherently sensitive to the number of samples available, and the effect of sample size on the observed and simulated Kendall's τ correlation coefficients is displayed in Figures S9–S11 of Supporting Information S1. Lastly, our analysis was based only on the 360-min interval with maximum precipitation. We have evaluated the statistics of events in which the maximum 10-, 30-, 60-, and 180-min precipitation volumes of an event do not fall within the maximum 360-min precipitation volume interval. This is the case for 25 events in the data set, among which only 5 events have a lower return period on the 360-min precipitation volume interval than on the other intervals. Additionally, these events have relatively short return periods of 2 years or less. Therefore, performing the analysis only on the maximum 360-min precipitation volume

interval does not exclude any extreme event. This might however not be the case in different climates, where the time windows of maximum 360-min precipitation volumes might not usually coincide with the time windows of shorter-duration maximum precipitation volumes (e.g., Villalobos Herrera et al., 2024).

We also analyze the confidence interval presented in Table 1, and how it evolves with sample size (Figure S12 in Supporting Information S1). The confidence interval is defined as the range between the 1st and 99th percentiles of the relative difference of total storm volume between design storms adopting the entire IDF curve (e.g., CDS or standard Euler type II design storm) and design storms with conditional constraining volume sampled from the copula. We find that the confidence interval is larger for lower conditional return periods (e.g., the confidence interval is larger for a 10-min, 5-year constraining volume than for a 10-min, 100-year constraining volume, Table 1). Additionally, the confidence interval is larger when the conditional sampling is applied to lower durations than when it is applied over longer durations (e.g., the confidence interval is higher for a 10-min, 5-year constraining volume than for a 60-min, 5-year constraining volume). When the conditional return period is lower than or equal to 20 years, the total storm volume of the simulated design storms can be either lower than (positive values in Table 1), higher than (negative values in Table 1), or equal to the total storm volume of design storms following the entire IDF curve. For conditional return periods larger than 20 years, the total storm volumes of the simulated design storms never exceed the volumes of design storms following the entire IDF curve. Regardless of the conditional return period and of the duration on which the condition is applied (except for the 360-min duration interval), the variability in possible duration-frequency samples indicates that a range of design storm events should ideally be used to ensure a robust risk assessment. In Figure S12 of Supporting Information S1, we analyze how the confidence interval evolves with sample size by showing the mean, 1st quartile, and 3rd quartile of the confidence interval size for 100 realizations and for sample sizes ranging from 10 to 10,000. We find that the mean confidence interval over 100 realizations remains fairly constant for sample sizes from 100 to 10,000, regardless of the applied conditional sampling. This suggests that a sample size of 100 design storms would allow capturing the range of variability.

To estimate the effect of different marginal distributions of precipitation on the vine copula outputs, we applied the Gamma and Lognormal distributions as they are widely used in precipitation modeling (Liu et al., 2011). The choice of marginal distribution is viewed as a parameter defined by the user. In regions with distinct precipitation characteristics, other statistical distributions that better fit the precipitation patterns can be selected. The marginal distributions of precipitation volumes may also vary across different durations if their associated volumes follow distinct distributions. Alternatively, the empirical marginal distributions can be used, but these would prevent the sampling of precipitation volumes beyond the maximum record in the observations. A hybrid approach combining parametric and empirical distributions may also be considered (Bevacqua et al., 2017).

We have adopted an IDF curve estimation based on the univariate statistical analysis of the precipitation events. Recognizing the complexity of precipitation events and the intra-event intensity relations highlights that this definition of the IDF curve has some limitations. However, considering its simplicity, its wide use, and that the results of this study were derived based on the marginal distribution and joint probabilities related to the precipitation volumes only, this shortcoming does not influence the proposed methodology.

Recent research has demonstrated that design infrastructure standards are challenged by the conventional sampling of design storm statistics, which assumes stationarity in precipitation events. This is partly due to the intensification of extreme precipitation events under a changing climate (Ebers et al., 2024; Lopez-Cantu & Samaras, 2018; Peleg et al., 2022; Wright et al., 2021). In response, methods for estimating nonstationary IDF estimates have been developed (Cheng & AghaKouchak, 2014; Marra et al., 2024; B. Zhang et al., 2022). These approaches could be combined with the presented method to adjust precipitation intensities for future climate conditions. A similar framework was applied by Peleg et al. (2024), where the CDS was re-parameterized for climate change by estimating future IDF curves using the TENAX model, which incorporates temperature as a covariate to project the changes in extreme sub-hourly precipitations. Along with precipitation intensities, the temporal distribution of precipitation within storms has been recognized as having a large impact on flood hazards and as being influenced by climate change (Hettiarachchi et al., 2018; Nathan et al., 2016; Villalobos Herrera et al., 2024; Visser et al., 2023). Consequently, the joint return period occurrence within precipitation events and the parameters of the constrained micro-canonical cascade model could change in the future. This should be explored in future research.

The model's code presented here is open-access, easy to implement, and user-friendly. This resource could be valuable for engineering companies and practitioners as it offers an opportunity for deriving new design storm profiles to supersede the current oversimplified design storm derivation methods, such as block methods. By accounting for the observed return period co-occurrences, the model can help mitigate the risk of under- or overestimation in flood hazard evaluation, ultimately leading to improved flood risk management.

6. Conclusion

We have presented a new method, based on vine copula and micro-canonical cascade model, for generating design storms that account for the co-occurrence of multiple return periods over different durations within a precipitation event. The simulated precipitation events reproduce observed duration-frequency dependencies, providing a more realistic approach than traditional design storm models. Using data from multiple stations in the city of Zurich, we demonstrated the model's capabilities and discussed its limitations and potential development in the future. The model's flexibility allows for application to user-defined precipitation durations, and the use of a non-parametric copula can capture various dependencies. Along with the source code, we provide an example of how the model can be used.

Data Availability Statement

The model codes, with the embedded example of precipitation for the city of Zurich presented above, are made freely accessible on a Zenodo repository (Cache, 2025). The model was implemented in MATLAB R2020b.

Acknowledgments
TC and NP were supported by the Swiss National Science Foundation (SNSF), Grant 194649 ("Rainfall and floods in future cities"). EB received funding from the Deutsche Forschungsgemeinschaft via the Emmy Noether Programme (Grant ID 524780515). The scientific colormaps (Crameri, 2018) were used in some figures.

References

Aas, K., Czado, C., Frigessi, A., & Bakken, H. (2009). Pair-copula constructions of multiple dependence. *Insurance: Mathematics and Economics*, *44*(2), 182–198. https://doi.org/10.1016/j.insmatheco.2007.02.001

Arnbjerg-Nielsen, K., Willems, P., Olsson, J., Beecham, S., Pathirana, A., Gregersen, I. B., et al. (2013). Impacts of climate change on rainfall extremes and urban drainage systems: A review. *Water Science and Technology*, *68*(1), 16–28. https://doi.org/10.2166/wst.2013.251

Bedford, T., & Cooke, R. M. (2002). Vines—A new graphical model for dependent random variables. *Annals of Statistics*, *30*(4), 1031–1068. https://doi.org/10.1214/aos/1031689016

Bevacqua, E., Maraun, D., Hobæk Haff, I., Widmann, M., & Vrac, M. (2017). Multivariate statistical modelling of compound events via pair-copula constructions: Analysis of floods in Ravenna (Italy). *Hydrology and Earth System Sciences*, *21*(6), 2701–2723. https://doi.org/10.5194/hess-21-2701-2017

Cache, T. (2025). Realistic design storm model. [Code]. *Zenodo*. https://doi.org/10.5281/zenodo.15119797

Cheng, L., & AghaKouchak, A. (2014). Nonstationary precipitation intensity-duration-frequency curves for infrastructure design in a changing climate. *Scientific Reports*, *4*(1), 7093. https://doi.org/10.1038/srep07093

Chow, V. T., Maidment, D. R., & Mays, L. W. (1988). *Applied hydrology*. McGraw-Hill.

Crameri, F. (2018). Scientific colour maps. *Zenodo*. https://doi.org/10.5281/zenodo.1243862

Cristiano, E., Veldhuis, M. C. T., & Giesen, N. V. D. (2017). Spatial and temporal variability of rainfall and their effects on hydrological response in urban areas—A review. *Hydrology and Earth System Sciences*, *21*(7), 3859–3878. https://doi.org/10.5194/hess-21-3859-2017

De Michele, C., & Salvadori, G. (2003). A generalized Pareto intensity-duration model of storm rainfall exploiting 2-copulas. *Journal of Geophysical Research*, *108*(D2). https://doi.org/10.1029/2002jd002534

Derx, J., Müller-Thomy, H., Kılıç, H., Cervero-Arago, S., Linke, R., Lindner, G., et al. (2023). A probabilistic-deterministic approach for assessing climate change effects on infection risks downstream of sewage emissions from CSOS. *Water Research*, *247*, 120746. https://doi.org/10.1016/j.watres.2023.120746

DWA-A 118. (2006). DWA-A 118: Hydraulische Bemessung und Nachweis von Entwässerungssystemen. *Hennef*.

Ebers, N., Schröter, K., & Müller-Thomy, H. (2024). Estimation of future rainfall extreme values by temperature-dependent disaggregation of climate model data. *Natural Hazards and Earth System Sciences*, *24*(6), 2025–2043. https://doi.org/10.5194/nhess-24-2025-2024

Fontanazza, C. M., Freni, G., Loggia, G. L., & Notaro, V. (2011). Uncertainty evaluation of design rainfall for urban flood risk analysis. *Water Science and Technology*, *63*(11), 2641–2650. https://doi.org/10.2166/wst.2011.169

Fowler, H. J., Lenderink, G., Prein, A. F., Westra, S., Allan, R. P., Ban, N., et al. (2021). Anthropogenic intensification of short-duration rainfall extremes. *Nature Reviews Earth & Environment*, *2*, 107–122. https://doi.org/10.1038/s43017-020-00128-6

Grimaldi, S., & Serinaldi, F. (2006). Design hyetograph analysis with 3-copula function. *Hydrological Sciences Journal*, *51*(2), 223–238. https://doi.org/10.1623/hysj.51.2.223

Güntner, A., Olsson, J., Calver, A., & Gannon, B. (2001). Cascade-based disaggregation of continuous rainfall time series: The influence of climate. *Hydrology and Earth System Sciences*, *5*(2), 145–164. https://doi.org/10.5194/hess-5-145-2001

Hall, P., Wolff, R. C., & Yao, Q. (1999). Methods for estimating a conditional distribution function. *Journal of the American Statistical Association*, *94*(445), 154–163. https://doi.org/10.1080/01621459.1999.10473832

Hettiarachchi, S., Wasko, C., & Sharma, A. (2018). Increase in flood risk resulting from climate change in a developed urban watershed—The role of storm temporal patterns. *Hydrology and Earth System Sciences*, *22*(3), 2041–2056. https://doi.org/10.5194/hess-22-2041-2018

Huff, F. A. (1967). Time distribution of rainfall in heavy storms. *Water Resources Research*, *3*(4), 1007–1019. https://doi.org/10.1029/wr003i004p01007

Huff, F. A. (1975). Urban effects on the distribution of heavy convective rainfall. *Water Resources Research*, *11*(6), 889–896. https://doi.org/10.1029/wr011i006p00889

Keifer, C. J., & Chu, H. H. (1957). Synthetic storm pattern for drainage design. *Journal of the Hydraulics Division*, *83*(4), 1–25. https://doi.org/10.1061/jyceaj.0000104

Krvavica, N., & Rubinic, J. (2020). Evaluation of design storms and critical rainfall durations for flood prediction in partially urbanized catchments. *Water*, *12*(7), 2044. https://doi.org/10.3390/w12072044

Kundzewicz, Z. W., Kanae, S., Seneviratne, S. I., Handmer, J., Nicholls, N., Peduzzi, P., et al. (2014). Flood risk and climate change: Global and regional perspectives. *Hydrological Sciences Journal*, *59*, 1–28. https://doi.org/10.1080/02626667.2013.857411

Li, J., Zhu, X., Lee, C.-F., Wu, D., Feng, J., & Shi, Y. (2015). On the aggregation of credit, market and operational risks. *Review of Quantitative Finance and Accounting*, *44*(1), 161–189. https://doi.org/10.1007/s11156-013-0426-0

Lisniak, D., Franke, J., & Bernhofer, C. (2013). Circulation pattern based parameterization of a multiplicative random cascade for disaggregation of observed and projected daily rainfall time series. *Hydrology and Earth System Sciences*, *17*(7), 2487–2500. https://doi.org/10.5194/hess-17-2487-2013

Liu, Y., Zhang, W., Shao, Y., Kexin, Z., Liu, C., Zhang, W. C., & Zhang, K. X. (2011). A comparison of four precipitation distribution models used in daily stochastic models. *Advances in Atmospheric Sciences*, *28*(4), 809–820. https://doi.org/10.1007/s00376

Lopez-Cantu, T., & Samaras, C. (2018). Temporal and spatial evaluation of storm water engineering standards reveals risks and priorities across the United States. *Environmental Research Letters*, *13*(7), e2019GL086797. https://doi.org/10.1088/1748-9326/aac696

Marra, F., Koukoula, M., Canale, A., & Peleg, N. (2024). Predicting extreme sub-hourly precipitation intensification based on temperature shifts. *Hydrology and Earth System Sciences*, *28*(2), 375–389. https://doi.org/10.5194/hess-28-375-2024

Müller, H., & Haberlandt, U. (2018). Temporal rainfall disaggregation using a multiplicative cascade model for spatial application in urban hydrology. *Journal of Hydrology*, *556*, 847–864. https://doi.org/10.1016/j.jhydrol.2016.01.031

Müller-Thomy, H. (2020). Temporal rainfall disaggregation using a micro-canonical cascade model: Possibilities to improve the autocorrelation. *Hydrology and Earth System Sciences*, *24*(1), 169–188. https://doi.org/10.5194/hess-24-169-2020

Nagler, T., Schellhase, C., & Czado, C. (2017). Nonparametric estimation of simplified vine copula models: Comparison of methods. *Dependence Modeling*, *5*(1), 99–120. https://doi.org/10.1515/demo-2017-0007

Nathan, R., Stephens, D., Smith, M., Jordan, P., Scorah, M., Shepherd, D., et al. (2016). Impact of natural variability on design flood flows and levels. In *Proceedings of the 37th hydrology and water resources symposium 2016: Water, infrastructure and the environment* (pp. 335–345). https://doi.org/10.3316/informit.688989822440058

Nelsen, R. B. (2006). *An introduction to copulas*. Springer Science & Business Media.

Olsson, J. (1998). Evaluation of a scaling cascade model for temporal rainfall disaggregation. *Hydrology and Earth System Sciences*, *2*(1), 19–30. https://doi.org/10.5194/hess-2-19-1998

Onof, C., Faulkner, D., & Wheater, H. S. (1996). Design rainfall modelling in the Thames catchment. *Hydrological Sciences Journal*, *41*(5), 715–733. https://doi.org/10.1080/02626669609491541

Peleg, N., Ban, N., Gibson, M. J., Chen, A. S., Paschalis, A., Burlando, P., & Leitao, J. P. (2022). Mapping storm spatial profiles for flood impact assessments. *Advances in Water Resources*, *166*, 104258. https://doi.org/10.1016/j.advwatres.2022.104258

Peleg, N., Blumensaat, F., Molnar, P., Fatichi, S., & Burlando, P. (2017). Partitioning the impacts of spatial and climatological rainfall variability in urban drainage modeling. *Hydrology and Earth System Sciences*, *21*(3), 1559–1572. https://doi.org/10.5194/hess-21-1559-2017

Peleg, N., Wright, D. B., Fowler, H. J., Leitão, J. P., Sharma, A., & Marra, F. (2024). A simple and robust approach for adapting design storms to assess climate-induced changes in flash flood hazard. *Advances in Water Resources*, *193*, 104823. https://doi.org/10.1016/j.advwatres.2024.104823

Ribeiro, A. F. S., Russo, A., Gouveia, C. M., Páscoa, P., & Zscheischler, J. (2020). Risk of crop failure due to compound dry and hot extremes estimated with nested copulas. *Biogeosciences*, *17*(19), 4815–4830. https://doi.org/10.5194/bg-17-4815-2020

Sklar, A. (1959). Fonctions de répartition à n dimension et leurs marges. *Institut Statistique de l'Université Paris*, *8*, 229–231.

Vandenberghe, S., Verhoest, N. E., Buyse, E., & Baets, B. D. (2010). A stochastic design rainfall generator based on copulas and mass curves. *Hydrology and Earth System Sciences*, *14*(12), 2429–2442. https://doi.org/10.5194/hess-14-2429-2010

Viglione, A., & Blöschl, G. (2009). On the role of storm duration in the mapping of rainfall to flood return periods. *Hydrololgy and Earth System Sciences*, *13*, 205–216. https://doi.org/10.5194/hess-13-205-2009

Villalobos Herrera, R., Blenkinsop, S., Guerreiro, S. B., Dale, M., Faulkner, D., & Fowler, H. J. (2024). Towards new design rainfall profiles for the United Kingdom. *Journal of Flood Risk Management*, *17*(1), e12958. https://doi.org/10.1111/jfr3.12958

Visser, J. B., Wasko, C., Sharma, A., & Nathan, R. (2023). Changing storm temporal patterns with increasing temperatures across Australia. *Journal of Climate*, *36*(18), 6247–6259. https://doi.org/10.1175/JCLI-D-22-0694.1

Watt, E., & Marsalek, J. (2013). Critical review of the evolution of the design storm event concept. *Canadian Journal of Civil Engineering*, *40*(2), 105–113. https://doi.org/10.1139/cjce-2011-0594

Wright, D. B., Samaras, C., & Lopez-Cantu, T. (2021). Resilience to extreme rainfall starts with science. *Bulletin of the American Meteorological Society*, *102*(4), E808–E813. https://doi.org/10.1175/BAMS-D-20-0267.1

Zhang, B., Wang, S., Moradkhani, H., Slater, L., & Liu, J. (2022). A vine copula-based ensemble projection of precipitation intensity–duration–frequency curves at sub-daily to multi-day time scales. *Water Resources Research*, *58*(11), e2022WR032658. https://doi.org/10.1029/2022wr032658

Zhang, Y., Kim, C.-W., Beer, M., Dai, H., & Soares, C. G. (2018). Modeling multivariate ocean data using asymmetric copulas. *Coastal Engineering*, *135*, 91–111. https://doi.org/10.1016/j.coastaleng.2018.01.008